Mid-ocean ridge eruptions as a climate valve

Maya Tolstoy

Lamont-Doherty Earth Observatory of Columbia University, 61 Route 9W, Palisades, NY 10864-8000, U.S.A.

[1] Seafloor eruption rates, and mantle melting fueling eruptions, may be influenced by sea-level and crustal loading cycles at scales from fortnightly to 100 kyr. Recent mid-ocean ridge eruptions occur primarily during neap tides and the first 6 months of the year, suggesting sensitivity to minor changes in tidal forcing and orbital eccentricity. An ~100 kyr periodicity in fast-spreading seafloor bathymetry, and relatively low present-day eruption rates, at a time of high sea-level and decreasing orbital eccentricity suggest a longer term sensitivity to sea-level and orbital variations associated with Milankovitch cycles. Seafloor spreading is considered a small but steady contributor of CO_2 to climate cycles on the 100 kyr time scale, however this assumes a consistent short-term eruption rate. Pulsing of seafloor volcanic activity may feed back into climate cycles, possibly contributing to glacial/inter-glacial cycles, the abrupt end of ice ages, and dominance of the 100 kyr cycle.

1. Introduction

[2] The driving forces behind ice age cycles are hotly debated. In particular, the abrupt end of ice ages and dominance of the 100 kyr signal in climate cycles are not well understood [e.g. Shackleton, 2000; EPICA community members, 2004]. Orbital eccentricity, which ties closely to the 100 kyr signal, is a relatively small forcing in terms of insolation, and thus its association with the largest peaks in CO_2 is unexpected. Seafloor spreading is generally viewed as a steady-state process on the 100 kyr time scale. While some episodicity has been noted in seafloor bathymetry [e.g. Vogt et al., 1969; Kappel & Ryan, 1986], only long-term variations in spreading rate having been proposed to influence atmospheric CO_2 over the last 100 million years [Berner et al.,

1983; Miller et al., 2005]. Changes in hydrothermal output due to plate reorganization have also been proposed to cause significant flux changes in CO_2 on the 10's of millions of years time-scale [Owen & Rea, 1985], however major plate reorganizations are rare.

[3] Seafloor eruptions contribute to ocean CO_2 fluxes without the global cooling effect associated with terrestrial eruptions due to volcanic particles injected into the atmosphere [e.g. Robock, 2000]. However, until recently very little was known about mid-ocean ridge eruptions because most occur far from land, at seismicity levels below the detection capabilities of global seismic networks. Recent advances in seafloor hydroacoustic monitoring have allowed the timing and character of seafloor eruptions to be studied, in particular at intermediate and fast spreading ridges, beginning in 1993 and 1996 respectively [Fox et al., 1993; 2001].

2. Timing of Mid-Ocean Ridge Volcanic Activity

[4] Microearthquakes at mid-ocean ridges, which are sensitive to tidal forcing, occur preferentially during times of maximum extensional stresses [Wilcock, 2001; Tolstoy et al., 2002; Stroup et al., 2007]. Terrestrial volcanism has also been shown in some locations to be sensitive to tidal periodicities [e.g. Johnston & Mauk, 1972], seasonal loading and unloading [e.g. Mason et al., 2004], glacial loading, unloading [e.g. Jull and McKenzie, 1996] and rate of unloading [e.g. Jellinek et al., 2004], as well as rate of climatically driven sea-level change [McGuire et al., 1997]. However, timing of volcanic activity with respect to tidal forcing at mid-ocean ridges has not previously been studied. To date, nine mid-ocean ridge eruptions/diking events have been well documented in terms of their timing, seismic character, and seafloor confirmation of likely magmatic

activity [Fox et al., 1995; Fox & Dziak, 1998; Dziak & Fox, 1999; Tolstoy et al., 1999; 2001; 2006; Bohnenstiehl et al., 2004; Dziak et al., 2004; 2012]. Figure 1 shows that eight out of nine of these best-documented mid-ocean ridge magmatic events occurred during lows in the fortnightly tidal modulations (neap tides). A Schuster test (Emter, 1997) shows statistically significant non-random distribution with respect to the fortnightly modulations of the tides (99%). This suggests that seafloor eruptions are particularly sensitive to prolonged tidal unloading and implies a system response time [Jupp et al., 2004] that is generally longer than the diurnal and semi-diurnal tidal fluctuations (Figure 2).

[5] An annual bias in eruption times is also evident (Figure 1) with all nine of these events occurring preferentially during the period of 'unloading' in the annual solid-earth tides, that is between the time of closest approach to the sun (early January) and the furthest point from the sun (early July), during which the influence of the sun on the tides is gradually decreasing. A further eruption can be added to this list where precise timing is not known, but can be confidently placed in the March-April time frame based on submersible observations (Haymon et al., 1993), making the ten observations statistically significant (Schuster Test, 96%). This may reflect a long-wavelength sensitivity of melting at depth, melt transport and/or dike formation, due to lithospheric/asthenopheric extension and unloading. The thin seafloor lithosphere in this extensional environment would make seafloor volcanism much more sensitive to deformation due to eccentricity compared to terrestrial settings. The apparent sensitivity of mid-ocean ridge magmatism to this relatively minor yearly orbital perturbation implies that it may also be sensitive to long-term orbital perturbations, thus linking seafloor volcanism to the Milankovitch

cycles observed so strongly in climate data. The eccentricity of Earth's orbit, which tracks the largest ~100 kyr climate cycle [Hayes et al., 1976], is the orbital variation that should produce the largest direct forcing on seafloor volcanism, since maximum eccentricity (0.06) corresponds to an ~18 million km difference in the point of closest and furthest approach to the sun, compared with 100-1000's of km differences in solar proximity caused by variations in orbital precession and obliquity. Increases in orbital eccentricity should have the effect of increasing this apparent annual seafloor volcanic forcing.

[6] Variations in sea-level associated with climatic cycles, and in particular ice ages, may similarly impact the rate of melting and volcanism throughout the world's oceans (Lund & Asimow, 2011). Sea-level fluctuations due to ice age cycles are on the order of 100 m on the 5,000 - 100,000 year time scale [e.g. Miller et al., 2005]. The decrease in sea-level (unloading), associated with an ice age would lead to an increase in oceanic mantle melting and an increase in seafloor volcanism. Similarly, an increase in sea-level (loading) would have the opposite effect, suppressing melting in the mantle for some time. The deformation due to sea-level changes needs to be considered in combination with deformation associated with variations in orbital eccentricity as well as considering system response times.

[7] The time scale for the response of the seafloor and mantle is dependent on the rate of loading or unloading, the lithospheric thickness and asthenospheric viscosity. How fluctuations in melting feed back into dike initiation and eruption rates is also dependent on unloading rate. The mechanism of melt transport through the mantle is not well understood [e.g. Phipps Morgan & Holtzman, 2005] and thus understanding the impact of varied lithospheric and asthenospheric deformation on melt transport is difficult.

Furthermore, current literature disagrees on the rate of melt transport in the mantle by as much as three orders of magnitude [Elliott, 2005]. Therefore it is difficult to accurately model the quantitative impact of sea-level changes combined with changes in orbital eccentricity both in terms of volume of melt, and in terms of system lag time. However, simple calculations based on upwelling rates and isostatic responses suggest that system lag time might be on the order of 100's to 1000's of years, and observations from terrestrial systems suggest lag times of ~1-11 kyr [Jull & MacKenzie, 1996; Jellinek et al., 2004]. Such times are broadly consistent with modeling of sea-level influence alone [Lund & Asimow, 2011], however this modeling suggests changes in magma flux would be least significant at fast-spreading ridges. The absence of strong peaks associated shorter period sea-level changes suggests magma flux at the SEPR may also be responding directly to 100 kyr orbital eccentricity changes.

[8] Since we are currently in a period of relatively high sea-level and lower orbital eccentricity (0.0167), a model proposing sensitivity to these forcings would predict that current rates of seafloor volcanism would be lower than expected from simple spreading rate calculations. Present day eruption data supports this hypothesis. Hydroacoustic monitoring at the East Pacific Rise [Fox et al., 1995], northern Mid-Atlantic Ridge [Smith et al., 2002], and Juan de Fuca Ridge [Fox et al., 1994] all show significantly fewer eruptions than would be predicted based on spreading rates and the assumption of 1 m of opening (dike width) per eruption (Supporting Text S1).

3. Bathymetric evidence for pulsing of seafloor volcanism

[9] Seafloor spreading would continue regardless of the stage of the climatic or orbital cycle. However, the sensitivity of melting and eruptions to loading and unloading from sea-level and orbital forcings would predict fluctuations in the amount of seafloor volcanism associated with this sustained spreading, particularly at the 100 kyr periodicity. Seafloor topography considered in terms of spreading rate may provide clues to fluctuations in magmatism over 10's of thousands of years. The Southern East Pacific Rise (SEPR) provides a site where faulting is least dominant, and magmatism is most prevalent. A period dominated by magmatism may have thicker crust, or shallower bathymetry, due to a thicker layer of surface extrusive volcanics (Layer 2A), and/or less thinning from faulting. A period of decreased eruptions, with fewer diking events, or fewer dikes that reached the surface, may have a thinner layer of extrusive volcanics, and/or more thinning due to faulting, resulting in deeper bathymetry. While a lag is predicted between forcings and eruptions, during voluminous eruptions it is common for lava to flow away from the axis 100’s of m’s to as much as 2 km, meaning that lava is built up on seafloor that is 1000’s to 10,000’s of years older than the eruption itself, thus perhaps counteracting the system lag in terms of seafloor appearance.

[10] At 17°S the SEPR is spreading at a full rate of ~14.7 cm/yr [Scheirer et al., 1996], and high-resolution bathymetric maps extend 100's of km off-axis. Figure 3A compares bathymetry for ~775 kyr of spreading on the western side of the SEPR at 17°S (Supporting Figure S1), with a ~800 kyr CO_2 time series from Antarctic ice-cores [Lüthi et al, 2008, and references therein], (which broadly follows sea-level at longer time periods), as well as orbital eccentricity [Varadi et al., 2003], which ties closely to the ~100 kyr periodicity in Milankovitch cycles. A visual comparison indicates correlation

between periods of low CO_2, low orbital eccentricity and periods of apparent decreased magmatism, as well as periods of abruptly increasing CO_2, and abruptly increasing magmatism, and high orbital eccentricity. An examination of the spectral energy of these data supports this interpretation, with peaks at a wavelength near 100 kyr for both the bathymetric, CO_2 and eccentricity data (Figure 3B). Normalized overlays of the bathymetry and CO2 (Supporting Figure S2) and bathymetry and eccentricity (Supporting Figure S3) further illustrate that the 100 kyr cycles appear to be broadly in phase.

4. Discussion and Conclusions

[11] There are several ways in which seafloor volcanism can contribute to global climate change. The first is the direct emission of CO_2 into the ocean that will eventually contribute to atmospheric levels through venting at upwelling sites. In addition to immediate release of greenhouse gases from seafloor eruptions, the subsequent increased high and low temperature hydrothermal venting may impact the CO_2 output. However, whether hydrothermal venting is a net source or sink of CO_2 is still unclear (e.g. Lang et al., 2006), due to paucity of measurements.

[12] Overall, the average annual contribution of CO_2 from seafloor spreading is generally considered to be small though not insignificant (~2 x 10^{12} mol/yr) [e.g. Resing et al., 2004] with respect to the global carbon cycle. However, this assumes a model of near continuous release, whereas a model of frequent pulses of activity followed by quiescent periods might result in more significant pulses of CO_2 into the global carbon

system. Approximately 2 km of glacial unloading in Iceland resulted in volcanism rates 20-30 times higher than today [Jull & McKenzie, 1996].

[13] Changes in sea-level of ~100 m and changes in the forcing from orbital eccentricity applied to the relatively thin oceanic lithosphere, across a broad area may result in a smaller but nevertheless significant pulsing of seafloor volcanism. The large spatial extent of mid-ocean ridges means that even a small increase in the melting and volcanism rate may have significant consequences for the global carbon budget. A CO_2 production rate of ~2 x 10^{12} mole/yr is ~0.088 gT/yr or ~0.041 ppmv of CO_2. For instance, an increase of only 50% in the eruption rate over the ~5 kyr typical for abrupt ends to ice-ages would thus theoretically result in an ~100 ppmv rise in CO_2. However, the transport of CO_2 from the seafloor to the atmosphere is physically and geochemically complex and likely only a fraction reaches the atmosphere (Huybers & Langmuir, 2009). The contribution of off-axis volcanism, submarine back-arc volcanism, and island arc volcanism, which would also be influenced by loading and unloading, may be an additional factor.

[14] This pulsing would provide a mechanism for seafloor volcanism to act as a negative climate feedback with respect to glaciation, but potentially a direct contributor to climate change through geophysical responses to changes in orbital eccentricity. Release of greenhouse gases would increase during periods of extreme glaciation and/or high orbital eccentricity, and decrease following periods of glacial melting and/or low orbital eccentricity. The glacial dependence is consistent with observations that ice-sheet volume lags CO_2 and temperature variations in 100 kyr ice age cycles [Shackleton, 2000]. While loading and unloading due to sea-level change is likely to influence melting

on the 1000's of years time scale, the timing of variations in eruption rates may also be influenced by orbital eccentricity as well as the variability in the rate of change of sea-level. Fluctuations in eruption rates may thus be a complex interplay of the forcings associated with sea-level, rate of change of sea-level, and orbital eccentricity, likely leading to short-term fluctuations on the 1000's of years time scale with a longer term ~100 kyr cycle superimposed.

[15] Estimates of the effect of seafloor spreading on the global carbon cycle and greenhouse gases are not well constrained, but are based largely on calculations that assume steady-state input from steady-state spreading. Seafloor bathymetry and present day sensitivity to tidal and orbital forcing indicate that this steady-state assumption may not be accurate on the time scale of cycles observed in climate variability (1000's to ~100,000 years). Instead, while seafloor spreading may be relatively constant on average, seafloor volcanism could be viewed as a highly variable process that may increase and decrease with climatic and orbital forcing, acting as a climatic valve that causes the flow of greenhouse gases to fluctuate.

5. Acknowledgements

[14] Data used here are available through the Marine Geoscience Data System (http://www.marine-geo.org/portals/gmrt/) and in references cited. This work was supported by NSF under grants OCE-0327283 , OCE-0732569, and OCE-0961594, as well as LDEO. I thank R.F. Anderson, W.S. Broecker, W.R. Buck, T.J. Crone, A.M. Jellinek, B. Liepert, W.R. McGillis, R. Newton and D. Peteet for many useful discussions and comments on the manuscript. I thank E.T. Baker for an early particularly constructive

and thoughtful review. I also thank P. Vogt and P. Huyber for reviews that improved the manuscript.

References

Berner, R.A., A.C. Lasaga, and R.M. Garrels (1983), The carbonate-silicate geochemical cycle and its effect on atmospheric carbon dioxide over the past 100 million years, Amer. J. Sci., 283, 641-683.

Bohnenstiehl, D.R., R.P. Dziak, M. Tolstoy, C. Fox, and M. Fowler (2004), Temporal and Spatial History of the 1999-2000 Endeavour Seismic Series, Juan de Fuca Ridge, Geochem. Geophys. Geosys. 5, doi:10.1029/2004GC000735.

Dziak, R.P., and C.G. Fox (1999), The January 1998 earthquake swarm at axial volcano, Juan de Fuca Ridge: Hydroacoustic evidence of seafloor volcanic activity, Geophys. Res. Lett., 26, 3429-3432.

Dziak, R.P., D. Smith, D. Bohnenstiehl, C. Fox, D. Desbruyeres, H. Matsumoto, M. Tolstoy, and D. Fornari (2004), Evidence of a recent magma dike intrusion at the slow-spreading Lucky Strike segment, Mid-Atlantic Ridge, J. Geophys. Res., 109, doi:10.1029/2004JB003141.

Dziak, R.P., J.H. Haxel, D.R. Bohnenstiehl, W.W. Chadwick, S.L. Nooner, M.J. Fowler, H. Matsumoto, and D.A. Butterfied (2012),Seismic precursors and magma ascent before the April 2011 eruption at Axial Seamount, Nature Geoscience, 5, doi: 10.1038/ngeo1490.

Elliott, T. (2005), Earth science – Unleaded high-performance, Nature, 437, doi: 10.1038/437485a.

EPICA community members (2004), Eight glacial cycles from an Antarctic ice core, Nature, 429, 623-628.

Fox, C.G., R.P. Dziak, H. Matsumoto, and A.E. Schreiner (1993), Potential for monitoring low-level seismicity on the Juan de Fuca Ridge using military hydrophone arrays, Mar. Tech. Soc., 27, 22-29.

Fox, C.G., W.E. Radford, R.P. Dziak, T.K. Lau, H. Matsumoto, A.E. Schreiner (1995), Acoustic detection of a sea-floor spreading episode on the Juan-de-Fuca Ridge using military hydrophone arrays, Geophys. Res. Lett., 22, 131-134.

Fox, C.G., and R.P. Dziak (1998), Hydroacoustic detection of volcanic activity on the Gorda Ridge, February-March 1996, Deep-Sea Res. II, 12, 2513-2530.

Fox, C.G., H. Matsumoto, and T.-K. Lau (2001), A. Monitoring Pacific Ocean seismicity from an autonomous hydrophone array, J. Geophys. Res., 106, 4183-4206.

Haymon, R.M., D.J. Fornari, K.L. Von Damm, M.D. Lilley, M.R. Perfit, J.M. Edmond, W.C. Shanks III, R.A. Lutz, J.B. Grebmeier, S. Carbotte, D. Wright, E. McLaughlin, E. Smith, N. Beedle, and E. Olson (1993), Volcanic eruption of the mid-ocean ridge along the East Pacific Rise crest at 9°45-52'N: Direct submersible observations of seafloor phenomena associated with an eruption event in April, 1991, Earth Planet. Sci. Lett., 11, 85-101.

Hays, J.D., J. Imbrie, and N.J. Shackleton (1976), Variations in the Earth's Orbit: Pacemaker of the Ice Ages, Science, 194, 1121-1132.

Huybers, P., C. Langmuir (2009), Feedback between deglaciation, volcanism, and atmospheric CO_2, Earth Planet. Sci. Lett., 286, 479-491.

Jellinek, A.M., M. Manga, and M.O. Saar (2004), Did melting glaciers cause volcanic eruptions in eastern California? Probing the mechanics of dike formation, J. Geophys. Res., 109, doi:10.1029/2004JB002978.

Johnston, M. J., and F.J. Mauk (1972), Earth Tides and the Triggering of Eruptions from Mt Stromboli, Italy, Nature, 239, 266-267.

Jull, M., and D. McKenzie (1996), The effect of deglaciation on mantle melting beneath Iceland, J. Geophys. Res., 101, 21815-21828.

Jupp, T.E., D.M. Pyle, B.G. Mason, and W.B. Dade (2004), A statistical model for the timing of earthquakes and volcanic eruptions influenced by periodic processes, J. Geophys. Res., 109, doi:10.1029/2003JB002584.

Kappel, E.S., and W.B.F. Ryan (1986), Volcanic Episodicity and a Non-Steady State Rift Valley Along Northeast Pacific Spreading Centers, J. Geophys. Res., 91, pp 13,925-13,940.

Lüthi, D., M. Le Floch, B. Bereiter, T. Blunier, J.-M. Barnola, U. Siegenthaler, D. Raynaud, J. Jouzel, H. Fischer, K. Kawamura, and T.F. Stocker (2008), High-resolution carbon dioxide concentration record 650,000-800,000 years before present, Nature, 453, 379-382.

Lund, D.C., and P.D. Asimow (2011), Does sea level influence mid-ocean ridge magmatism on Milankovitch timescales? Geochem. Geophys. Geosys. 12, doi:10.1029/2011GC003693.

Mason, B.G., D.M. Pyle, W.B. Dade, and T. Jupp (2004), Seasonality of volcanic eruptions. J. Geophys. Res. 109, doi:10.1029/2002JB002293.

Matsumoto, K.T., T. Takanezawa, and M. Ooe (2000), Ocean tide models developed by assimilating TOPEX/POSEIDON altimeter data in hydrodynamical model: A global model and a regional model around Japan, J. Oceanogr., 56, 567-581.

McGuire, W.J., R.J. Howarth, C.R. Firth, A.R. Solow, A.D. Pullen, S.J. Saunders, I.S. Stewart, and C. Vita-Finzi (1997), Correlation between rate of sea-level change and ency of explosive volcanism in the Mediterranean, Nature, 389, 473-476.

Miller, K.G., M.A. Kominz, J.V. Browning, J.D. Wright, G.S. Mountain, M.E. Katz, P.J. Sugarman, B.S. Cramer, N. Christie-Blick, and S.F. Pekar (2005), The Phanerozoic Record of Global Sea-Level Change, Science, 310, 1293-1298.

Owen, R.M., and D.K. Rea (1985), Seafloor Hydrothermal Activity Links Climate to Tectonics: The Eocene Carbon Dioxide Greenhouse, Science, 227, 166-169.

Phipps Morgan, J., and B.K. Holtzman (2005), Vug waves: A mechanism for coupled rock deformation and fluid migration, Geochem. Geophys. Geosys., 6, doi:10.1029/2004GC000818.

Resing, J.A., J.E. Lupton, R.A. Feely, and M.D. Lilley (2004), CO_2 and ^{3}He in hydrothermal plumes: implications for mid-ocean ridge CO_2 flux, Earth Planet. Sci. Lett., 226, 449-464.

Robock, A. (2000), Volcanic Eruptions and Climate, Rev. Geophys., 38, 191-219.

Scheirer, D.S., K.C. Macdonald, D.W. Forsyth, S.P. Miller, D.J. Wright, M.H. Cormier, and C.M. Weiland (1996), A map series of the Southern East Pacific Rise and its flanks, 15 degrees S to 19 degrees S, Mar. Geophys. Res., 18, 1-12.

Emter, D. (1997), Tidal triggering of earthquakes and volcanic events, in Tidal Phenomena, edited by S. Bhattacharji et al., pp. 293– 309, Springer, New York.

Shackleton, N.J. (2000), The 100,000-Year Ice-Age Cycle Identified and Found to Lag Temperature, Carbon Dioxide, and Orbital Eccentricity, Science, 289, 1897-1902.

Smith, D.K., M. Tolstoy, C.G. Fox, D.R. Bohnenstiehl, H. Matsumoto, and M. J. Fowler (2002), Hydroacoustic Monitoring of Seismicity at the Slow Spreading Mid-Atlantic Ridge, Geophys. Res. Lett., 29, doi:10.1029/2001GL013912.

Stroup, D., D.R. Bohnenstiehl, M. Tolstoy, F. Waldhauser, and R.T. Weekly (2007), The Pulse of the Seafloor: Tidal triggering of microearthquakes at 9˚50'N East Pacific Rise, Geophys. Res. Lett., 34, doi:10.1029/2007GL030088.

Tolstoy, M., D.J. Fornari, and C.J. Fox (1999), Detailed Investigation of T-phase Swarms on the East Pacific Rise, EOS Trans. AGU, 80, F1073.

Tolstoy, M., D.R. Bohnenstiehl, M. Edwards, and G. Kurras (2001), The seismic character of volcanic activity at the ultra-slow spreading Gakkel Ridge, Geology, 29, 1139-1142.

Tolstoy, M., F.L. Vernon, J.A. Orcutt, and F.K. Wyatt (2002), Breathing of the seafloor: Tidal correlations of seismicity at Axial volcano, Geology, 30, 503-506.

Tolstoy, M., J.P. Cowen, E.T. Baker, D.J. Fornari, K.H. Rubin, T.M. Shank, F. Waldhauser, D.R. Bohnenstiehl, D.W. Forsyth, R.C. Holmes, B. Love, M.R. Perfit, and R.T. Weekly (2006), A Seafloor Spreading Event Captured by Seismometers: Forecasting and Characterizing an eruption, Science, DOI: 10.1126/science.1133950/.

Varadi, F., B. Runnegar, and M. Ghil (2003), Successive refinements in long-term integrations of planetary orbits, Astrophys. J., 592, 620-630.

Vogt, P.R., O.E. Avery, E.D. Schneider, C.N. Anderson, and D.R. Bracey (1969), Discontinuities in Sea-floor Spreading, Tectonophyiscs, 8, pp 285-317.

Wilcock, W. S. D. (2001), Tidal triggering of micro earthquakes on the Juan de Fuca Ridge, Geophys. Res. Lett., 28, 3999-4002.

Figure 1: Mid-Ocean Ridge events confirmed to be magmatic/volcanic in origin through observations of fresh seafloor lava and/or changes in vent fluid chemistry (see main text for references). Event in grey on table (EPR 9N, 1991) was a confirmed eruption where the timing is known well enough to categorize the month, but not well enough to constraining fortnightly timing (Haymon et al., 1993). Red dots on the center plots indicate timing of initiation of magmatic activity with respect to ocean tides (sea surface height) [Matsumoto et al., 2000] at the location of the activity. Rose plot on the left shows distribution of events with respect to phase of the fortnightly modulations of the tides, based on the inflection points of an envelope function of the upper portion of the tidal cycle. All but one of the events happen near the low in fortnightly tides, with four happening just following the lowest point in the fortnightly modulations. Rose plot on the right shows the distribution of events with respect to the month of the year (or orbital eccentricity), with all events happening during the first six months of the year (increasing distance from the sun).

Figure 2: Cartoon illustrating the concept of the response time of the system [Jupp et al., 2004]. The load from the magma chamber is building through time (red line). For an eruption to occur the "load function" must exceed the "strength function" (blue line) of the overlying crust for a certain length of time ("response time"). When the load is near the failure point, tidal stress will be pushing the load alternately above and below the strength of the crust at diurnal and semi-diurnal intervals. However, if the response time

is greater than ~12-24 hours, the eruption would occur preferentially during the period of subdued tides, when the load function is more likely to consistently exceed the strength function for the required response time (days).

Figure 3: (A) Comparison of bathymetry from the Southern East Pacific Rise (SEPR) (red line), CO_2 records from Antarctic ice-cores (blue line) [Lüthi et al., 2008, and references therein], and orbital eccentricity (brown line) [Varadi et al., 2003]. Grey vertical bars indicate periods of high orbital eccentricity. The bathymetry is an average of nine ridge perpendicular lines on the western SEPR flank from17°21'S to 17°29'S (Supporting Figure S1) plotted versus age based on a half spreading rate of ~7.3 cm/yr [Scheirer et al., 1996] (Supporting Text S2). The bathymetry profiles were demeaned and filtered using a Butterworth high pass filter at 150 kyr to remove long-term lithospheric cooling trends. Periods of low and high CO_2 appear to be roughly in phase with periods of low and high crustal production, and low and high orbital eccentricity, particularly in the most recent glacial cycles where timing is most accurate. As the age of the seafloor increases, uncertainties in spreading rate compound, making timing of older bathymetric variations less robust. **(B)** Normalized periodogram of Antarctic ice-core CO_2 (blue), SEPR bathymetry (red) from (A), and eccentricity (brown) here also filtered at 150 kyr. Seafloor bathymetry exhibits clear peaks at ~96 kyr, ~71 kyr and ~55 kyr, with much smaller peaks at ~44 kyr and other higher frequencies. The CO2 and eccentricity data also show prominent peaks at ~95-96 kyr. CO2 shows some deflection at ~71 kyr relative to eccentricity and smaller peaks at higher frequencies. Eccentricity has a small peak at ~55 kyr. Note that due to uncertainties in absolute spreading rate, including the

assumption of consistent spreading rate over this time scale, true timing of peaks may be slightly different. Periodogram done using the Welch power spectral density method.

Figure 1

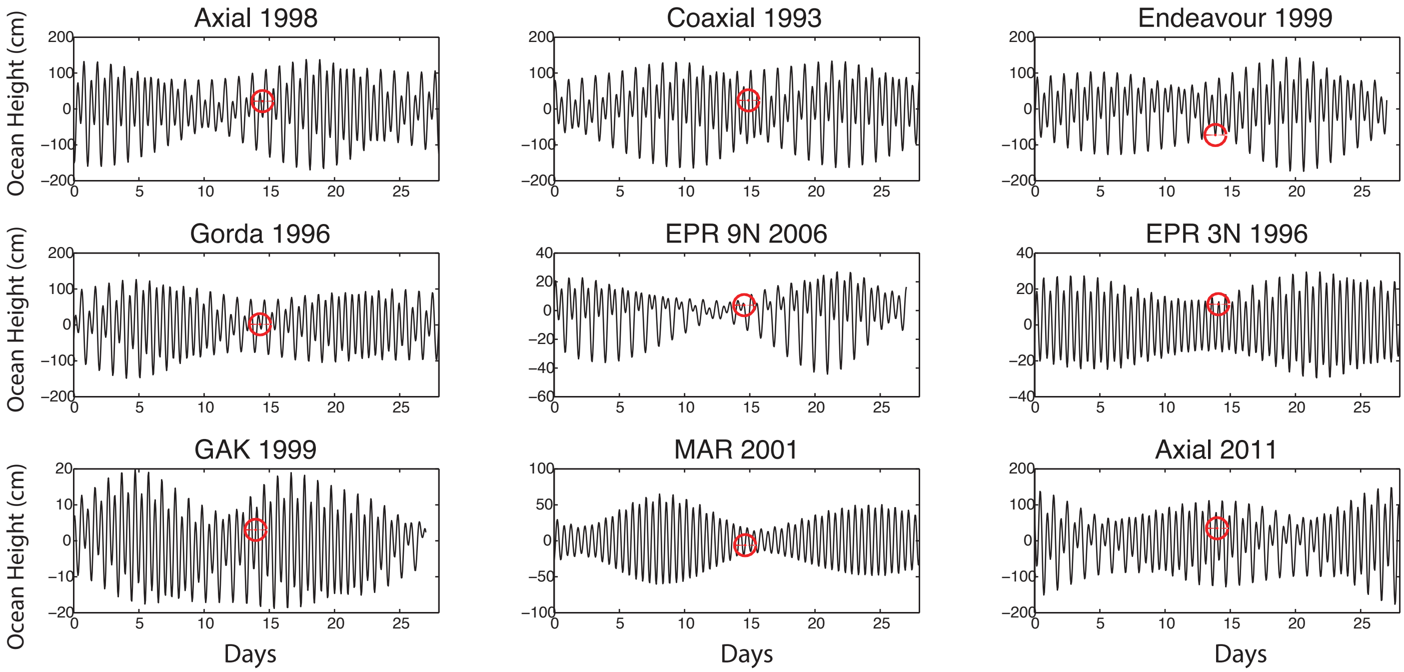

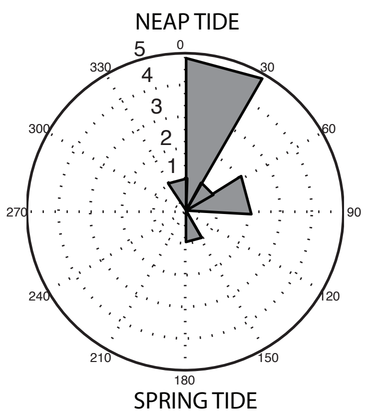

Site	Lat/Long	Year	Date Initiated
EPR 9N	9N/104W	1991	~April
Co-Axial	46N/129W	1993	June 26th
North Gorda	42N/126W	1996	February 28th
EPR 3N	3N/102W	1996	May 27th
Axial	46N/130W	1998	January 25th
Gakkel	85N/85E	1999	January 28th
Endeavor	48N/129W	1999	June 8th
MAR	37N/32W	2001	March 16th
EPR 9N	9N/104W	2006	January 22nd
Axial	46N/130W	2011	April 6th

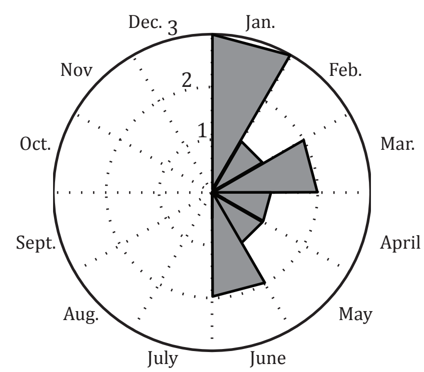

Figure 2

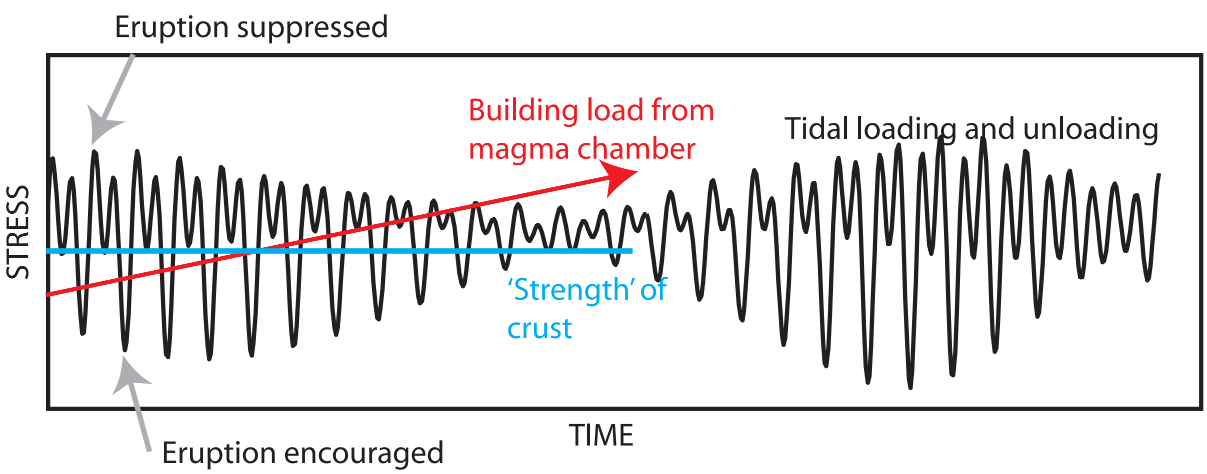
Eruption suppressed
Building load from
magma chamber
Tidal loading and unloading
STRESS
'Strength' of
crust
TIME
Eruption encouraged

Figure 3

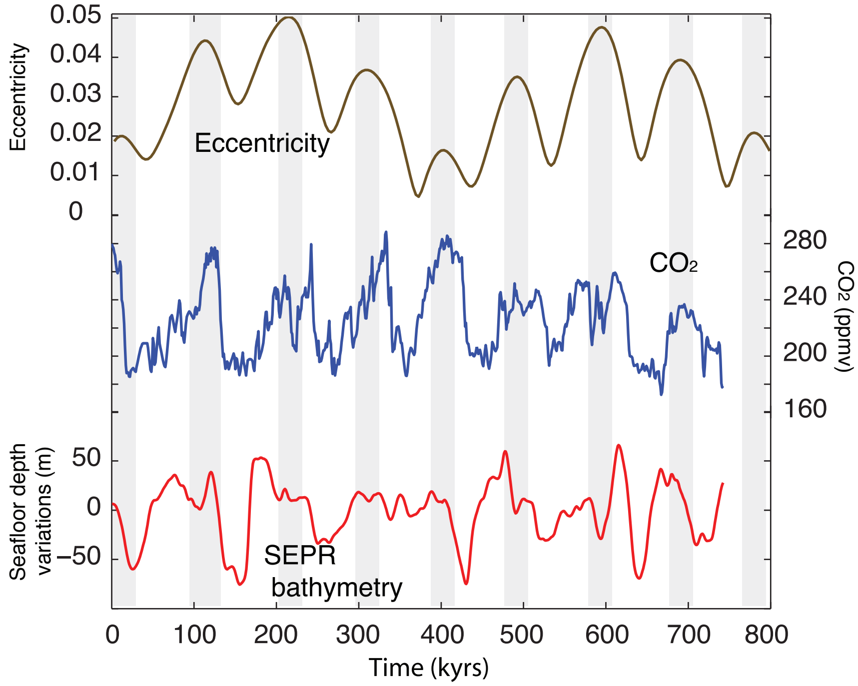

0.05
0.04
0.03
0.02
0.01
0
Eccentricity
Eccentricity
CO2
280
240
200
160
CO2 (ppmv)
Seafloor depth variations (m)
50
0
−50
SEPR bathymetry
0
100
200
300
400
500
600
700
800
Time (kyrs)

A

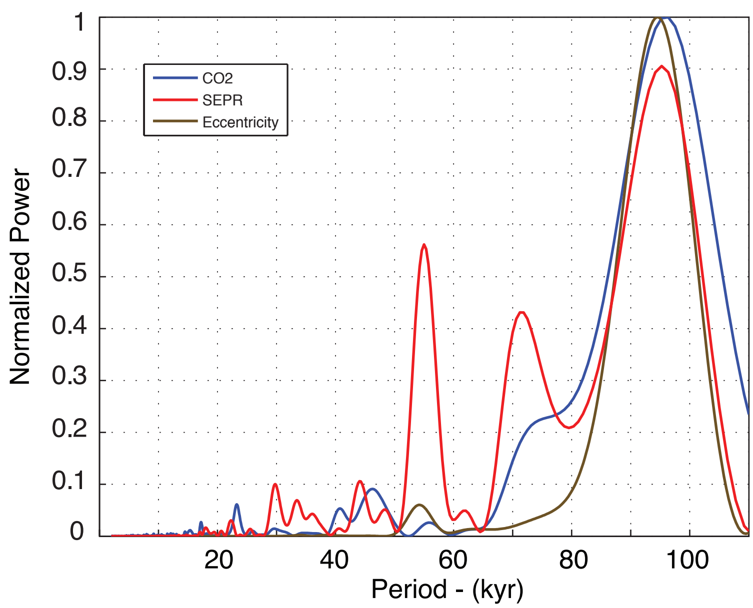

1
0.9
0.8
0.7
0.6
0.5
0.4
0.3
0.2
0.1
0
Normalized Power
CO2
SEPR
Eccentricity
20
40
60
80
100
Period - (kyr)

B

Geophysical Research Letters

Supporting Information for

Mid-ocean ridge eruptions as a climate valve

M.Tolstoy

Dept. of Earth and Environmental Sciences, Lamont-Doherty Earth Observatory of Columbia University, 61 Route 9W, Palisades, NY 10964-8000, USA (mt290@columbia.edu)

Contents of this file

Introduction

The supporting text provides a detailed explanation of the data that went into the calculation of present day eruption rates, as well as considerations in calculating the spreading rate for the SEPR from 17°21'S – 17°29'S. The figures provide a map of the SEPR 17°20'S-17°30'S area with the location of the bathymetric profiles shown. The figures also provide overlays of the relevant bathymetric, climate and eccentricity data along with cross-correlations.

Text S1.

Present Day Eruption Rates

Knowledge of the geographical distribution of seafloor eruptions comes primarily from hydroacoustic monitoring. This is geographically and temporally limited, but has been available at the Juan de Fuca Ridge (JdFR) since 1993 [Fox et al., 1993] (though with only intermittent recent coverage), the equatorial East Pacific Rise (EPR) (~10°S-10°N) since 1996

[Fox et al., 2001], and part of the northern Mid-Atlantic Ridge (MAR) (~15°N-35°N) from 1999 to 2004 [Smith et al., 2002; 2003], with some gaps in data due to instrument failure. At each site with prolonged monitoring, there have been fewer eruptions/magmatic events than would be predicted based on the spreading rate and an assumed 1 m dike width during eruptions.

Full spreading rates at the EPR between 10°N and 10°S are ~11 cm/yr to 14 cm/yr, which would predict that each segment would erupt every 7-9 years. However, the majority (~95%) of segments did not exhibit seismicity consistent with eruptions in ~10 years of monitoring [Fox et al., 2001; Tolstoy et al., 1999], let alone any repeat eruptions, as would have been predicted from the spreading rate. The only location where a repeat eruption has been documented [Tolstoy et al., 2006], due to a serendipitous discovery with Alvin [Haymon et al., 1993] prior to hydroacoustic monitoring, is at a segment centered at 9°50'N. The interval between eruptions was ~15 years at this site, or >50% longer than would be predicted.

On the MAR, where over 40 segments were monitored for ~5 years, a spreading rate of ~2.2-2.5 cm/yr would predict that each segment erupts once every 40-45 years, or on average one segment over the monitoring area would erupt each year. So while ~5 eruptions would have been predicted within the array during the observation period, no seismicity characteristic of magmatic activity was observed within the array [Smith et al., 2002, 2003] and the only definitive magmatic event observed was to the north of the array at the hot-spot influenced Lucky Strike Segment [Dziak et al., 2004].

At the JdFR with a spreading rate of ~5.9 cm/yr, an eruption would be expected every ~17 years. In the ~14 years of monitoring to date there have only been 4 segments (out of ~8) with confirmed magmatic events [Fox et al., 1995; Fox and Dziak, 1998; Dziak and Fox, 1999; Bohnenstiehl et al., 2004], and two of those have been in the proximity of the hotspot influenced Axial Volcano. While Axial Volcano itself has had two eruptions in ~13 years, it is obviously a high magmatic anomaly along the ridge system.

Therefore it can be inferred that based on the limited data available, we are currently in a period of reduced volcanic activity at mid-ocean ridges. However, on a geological time scale these data cover an extremely short time span, and the assumption of 1 m of spreading occurring with each eruption may be over simplified.

Text S2.

SEPR 17°S Spreading Rates

Note that spreading is thought to be asymmetric at this location, with the Western side spreading more slowly, and the half spreading rate is not predicted to be half the full spreading-rate (6.5 cm/yr vs. 7.35 cm/yr). Small errors in spreading rate compound with age in comparing bathymetric profiles to climate and eccentricity data. Correlation coefficients and statistical significance were found to be highest when using a half-spreading rate of 7.3 cm/yr (~half of the full rate) rather than the asymmetric rates predicted. These short term spreading rates are based on magnetic anomalies which are useful for long-term averages, but in the case of the last ~740,000 years (the length of the climate data compared) this is entirely within the Bruhnes period and thus defined by only one period of normal magnetic polarity.

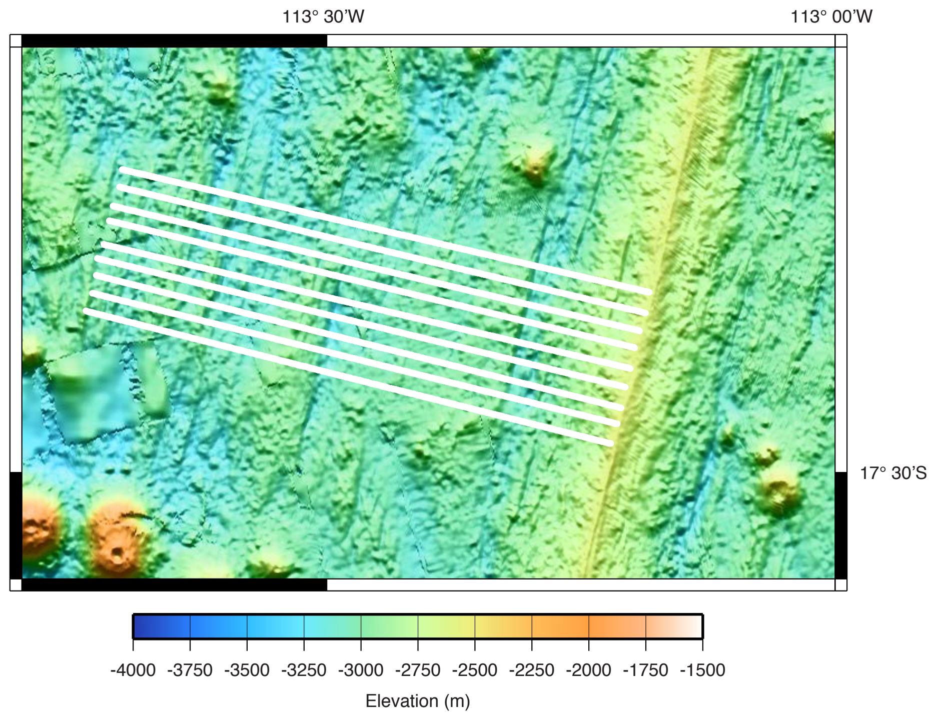

Figure S1. Map showing seafloor depth in the region of study, with white lines illustrating the location of the 9 tracks used to create the averaged bathymetric profile. By averaging 9 parallel tracks, smaller features specific to individual tracks, or ship-track artifacts are minimized. The site was chosen based on the existence of high resolution multibeam data, relatively few seamounts, and the absence of wakes from propagating ridges that would complicate dating.

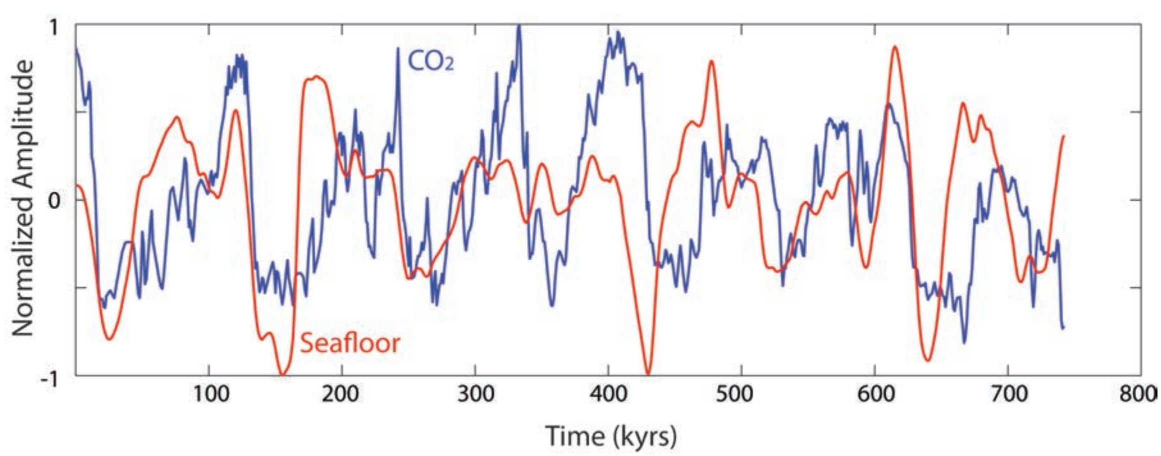

Figure S2. Bathymetric and climate (CO_2) data normalized to a maximum amplitude of 1, and superimposed.

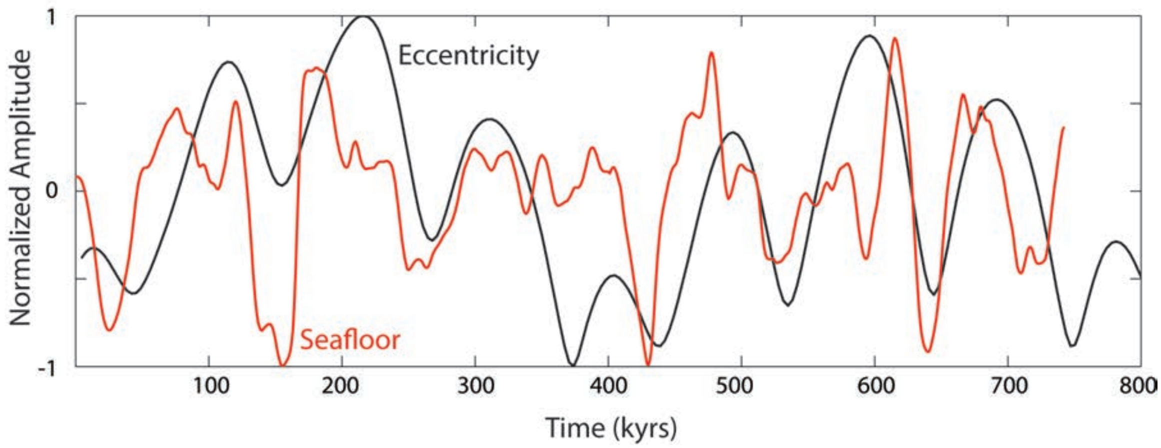

Figure S3. Bathymetric and Eccentricity data normalized to a maximum amplitude of 1, and superimposed.

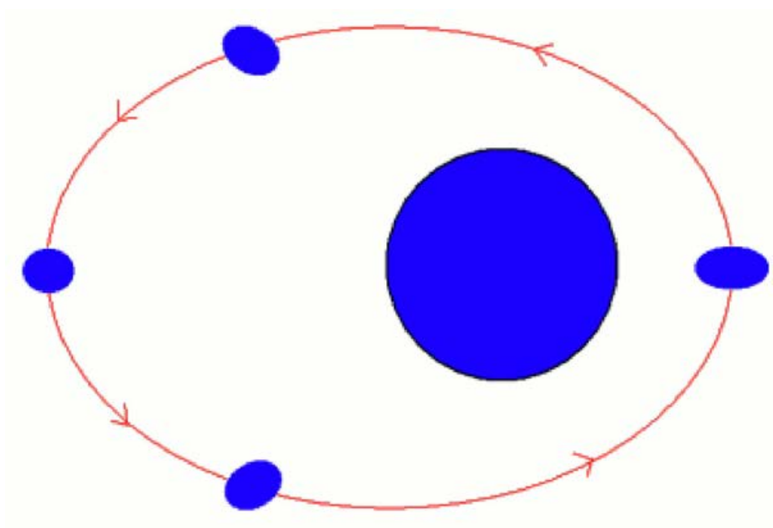

Figure S4. From response to reviewer:
Figure illustrates deformation of an orbiting body associated with orbital eccentricity.
Adapted from: http://large.stanford.edu/courses/2007/ph210/pavlichin2/
Early January is the to the right and early July is to the left (greatly exaggerated). In January the squeezing is maximized, but the impact of this on the stress field will vary as Earth rotates on its own axis. As Earth moves further away from the sun, there will be a relaxing of the squeezing stresses, and it appears that this is the most likely time for seafloor eruptions to occur.

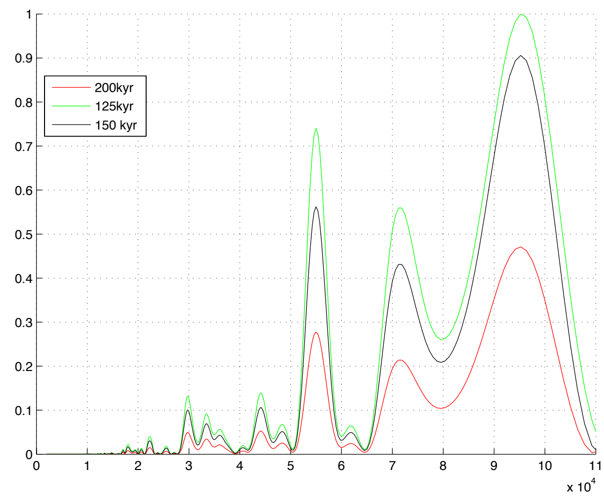

Figure S5. From response to reviewer:
In response to concerns about the filtering frequency equivalent to 125 kyr, a normalized periodogram of SEPR bathymetry is shown with filter frequencies equivalent to 125 kyr, 150 kyr and 200 kyr, to illustrate that the ~100 kyr peak remains.

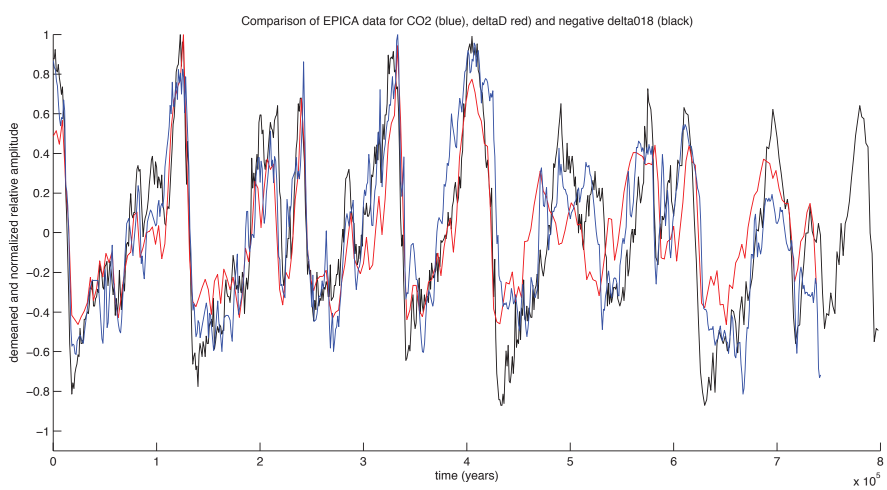

Figure S6. From response to reviewer:
A demeaned and normalized plot of CO2, delta-D and delta18O data from Antarctica cores [EPICA 2004, Lüthi et al., 2008], to illustrate that at the longer wavelengths of interest here, these three data types (and their proxies, including sea-level (delta18O)) broadly track each other.